Neutrino-nucleus reactions and muon capture in ^{12}C

F. Krmpotić,[1,2,3] A. Samana,[1] and A. Mariano[2,4]

[1]*Instituto de Física, Universidade de São Paulo, 05315-970 São Paulo-SP, Brazil*
[2]*Instituto de Física La Plata, CONICET, 1900 La Plata, Argentina*
[3]*Facultad de Ciencias Astronómicas y Geofísicas, Universidad Nacional de La Plata, 1900 La Plata, Argentina*
[4]*Departamento de Física, Universidad Nacional de La Plata, C. C. 67, 1900 La Plata, Argentina*

The neutrino-nucleus cross section and the muon-capture rate are discussed within a simple formalism that facilitates nuclear structure calculations. The corresponding formulas depend on only four types of nuclear matrix elements currently used in nuclear β decay. We have also considered nonlocality effects arising from the velocity-dependent terms in the hadronic current. We show that for both observables in ^{12}C the higher order relativistic corrections are of the order of $\sim$5% only and therefore do not play a significant role. As a nuclear model framework we use the projected quasiparticle random-phase approximation and show that the number projection plays a crucial role in removing the degeneracy between the proton-neutron two-quasiparticle states at the level of the mean field. Comparison is done with both the experimental data and the previous shell model calculations. The possible consequences of the present study on the determination of the $\nu_\mu \to \nu_e$ neutrino oscillation probability are briefly addressed.

I. INTRODUCTION

Semileptonic weak interactions with nuclei include a rich variety of processes, such as neutrino (antineutrino) scattering, charged lepton capture, and $e^\pm$ decays, and we have at our disposal the results of more than a half-century of exceptional experimental and theoretical work. At present the study of semileptonic weak interactions mainly focuses on possible exotic properties of the neutrino associated with its oscillations and massiveness by means of exclusive and inclusive scattering processes on nuclei, which are often used as neutrino detectors. An example is given by the recent experiments performed by both the LSND [1,2] and the KARMEN [3] Collaborations, looking for $\nu_\mu \to \nu_e$ and $\bar{\nu}_\mu \to \bar{\nu}_e$ oscillations with neutrinos produced by accelerators. When the ν_e's come from decay at rest (DAR) of μ^+'s the flux contains neutrinos with a maximum energy energy of 50 MeV and can be detected through both exclusive and inclusive $\nu_e + {}^{12}\text{C} \to {}^{12}\text{N} + e^-$ reactions [4]. For ν_μ's coming from the decay in flight (DIF) of π^+'s, the neutrino flux extends over the range (0, 300) MeV, and the $\nu_\mu \to \nu_e$ appearance mode is sought experimentally through the reaction $\nu_\mu + {}^{12}\text{C} \to {}^{12}\text{N} + \mu^-$, which also has been measured [5]. However, we do not have at our disposal experimental information on the ν_e reaction in the DIF energy range, which is necessary for evaluating the oscillation probabilities. Therefore, it is imperative to develop nuclear models, capable of reproducing the ν_e-DAR and ν_μ-DIF data, to be used to predict reliable values for the $\nu_e + {}^{12}\text{C} \to {}^{12}\text{N} + e^-$ cross section in the DIF energy range and to calibrate forthwith the $\nu_\mu \to \nu_e$ appearance probability. Needless to say, in addition and for consistence, the implemented model should also describe properly the well-known $^{12}\text{N} \to {}^{12}\text{C} + \nu_e + e^+$ β^+ decay and the $\mu^- + {}^{12}\text{C} \to \nu_\mu + {}^{12}\text{B}$ muon-capture modes.

The weak interaction formalism most frequently employed in the literature is that of Donnelly and Walecka [6,7], where the nuclear form factors are classified as Coulomb ($\mathcal{M}$), longitudinal ($\mathcal{L}$), transverse electric ($\mathcal{T}^{\text{el}}$), and transverse magnetic ($\mathcal{T}^{\text{mag}}$), in close analogy with the electromagnetic transitions. These factors, in turn, depend on seven nuclear matrix elements, denoted M_J^M, Δ_J^M, $\Delta_J'^M$, Σ_J^M, $\Sigma_J'^M$, $\Sigma_J''^M$, and Ω_J^M. However, in studying neutrino-induced reactions [8,9] it is sometimes preferred to employ the formulation of Kuramoto *et al.* [10], mainly because of its simplicity. The later formalism does not include the velocity-dependent terms in the hadronic current, and therefore the reaction cross section depends on only three nuclear form factors, denoted $|\langle f|\tilde{1}|i\rangle|^2$, $|\langle f|\tilde{\sigma}|i\rangle|^2$, and Λ. Moreover, the formalism of Kuramoto *et al.* [10] does not include the muon-capture rates. Therefore, to describe simultaneously the neutrino-nucleus reactions and muon-capture processes it is necessary to resort to additional theoretical developments, such as those of Luyten *et al.* [11] and Auerbach and Klein [12], where one uses the matrix elements M_V^2, M_A^2, and M_P^2, which are related to the former ones in a nontrivial way.

Quite recently, we have carried out a multipole expansion of the $V - A$ hadronic current, similar to the one used by Barbero *et al.* [13] for the neutrinoless double β decay, expressing all aforementioned observables in terms of the vector (V) and axial vector (A) nuclear form factors $\mathcal{M}_V$ and $\mathcal{M}_A^M$, with $M = -1, 0, +1$ [14]. Such a classification is closely related to the $V - A$ structure of the weak current and to the currently used nuclear β-decay formalisms, where the nuclear moments are expressed in a way that the *forbiddeness* of the transitions is easily recognized. This in no way means that we have developed a new theoretical framework; the final results can be found in one form or another in the literature. The main difference stems from the fact that we use the Racah algebra from the start, employing the spherical spatial coordinates instead of the Cartesian ones. Concomitantly, we also express the lepton trace in spherical coordinates, as done for instance in the book of Supek [15]. Here we present a few more details

than in Ref. [14] on the procedure we have followed and also consider first-order nonlocal corrections, which give rise to the additional matrix elements $\mathcal{M}_{V'}^M$ and $\mathcal{M}_{A'}$.

In Ref. [14] we have analyzed the inconveniences that appear in applying RPA-like models to describe the nuclear structure of the $\{^{12}\text{B}, ^{12}\text{C}, ^{12}\text{N}\}$ triad. We have established that the projected quasiparticle random-phase approximation (PQRPA) was the proper approach to treat both the short-range pairing and the long-range random-phase approximation (RPA) correlations. More details are given in the present work, putting special emphasis on the differences between the projected and the usual quasiparticle random-phase approximations. We also compare our PQRPA cross sections with recent shell model (SM) calculations [16,17] and analyze the reliability of the calculated energy dependence of the $\nu_e + ^{12}\text{C} \rightarrow ^{12}\text{N} + e^-$ cross section in the DIF energy region to be used in the evaluation of the oscillation probabilities.

The work will be organized as follows. In Sec. II we explain our multipole decomposition of the weak current and present the corresponding formulas for the neutrino-nucleus cross section and muon capture. In Sec. III we briefly overview the projected BCS (PBCS) and the PQRPA equations. The main reason for the latter is to emphasize the relationship with the usual QRPA, which is difficult to find in the existing literature. Finally, in Sec. IV we show the numerical results from the PQRPA model and compare them with the most recent SM calculations.

II. FORMALISM FOR THE WEAK INTERACTING PROCESSES

The weak Hamiltonian is expressed in the form [6,7,13,18]

$$H_W(\mathbf{r}) = \frac{G}{\sqrt{2}} J_\alpha l_\alpha e^{-i\mathbf{r}\cdot\mathbf{k}}, \qquad (2.1)$$

where $G = (3.04545 \pm 0.00006) \times 10^{-12}$ is the Fermi coupling constant (in natural units),

$$J_\alpha = i\gamma_4 \left[g_V\gamma_\alpha - \frac{g_M}{2\text{M}}\sigma_{\alpha\beta}k_\beta + g_A\gamma_\alpha\gamma_5 + i\frac{g_P}{\text{m}_\ell}k_\alpha\gamma_5 \right]$$
$$\equiv (\mathbf{J}, iJ_\emptyset) \qquad (2.2)$$

is the hadronic current operator,[1] and

$$l_\alpha = -i\overline{u}_{s_\ell}(\mathbf{p}, E_\ell)\gamma_\alpha(1 + \gamma_5)u_{s_\nu}(\mathbf{q}, E_\nu) \equiv (1, il_\emptyset) \quad (2.3)$$

is the plane-wave approximation for the matrix element of the leptonic current in the case of neutrino reactions. Here $\alpha, \beta = 1, 2, 3, 4$, and Walecka's notation [7] with the Euclidean metric for quadrivectors is employed (i.e., $x = \{\mathbf{x}, x_4 = ix_\emptyset\}$). The only difference is that we substitute his indices (0, 3) by our indices $(\emptyset, 0)$, which means that we use the index $\emptyset$ for the temporal component and the index 0 for the third spherical component. The quantity

$$k = P_i - P_f \equiv \{\mathbf{k}, ik_\emptyset\} \qquad (2.4)$$

is the momentum transfer, where P_i and P_f are momenta of the initial and final nucleon (nucleus), M is the nucleon mass, m_ℓ is the mass of the charged lepton, and g_V, g_A, g_M, and g_P are, respectively, the vector, axial-vector, weak-magnetism, and pseudoscalar effective dimensionless coupling constants. Their numerical values are

$$g_V = 1, \quad g_A = 1.26,$$
$$g_M = \kappa_p - \kappa_n = 3.70, \quad g_P = g_A\frac{2\text{M}\text{m}_\ell}{k^2 + \text{m}_\pi^2}. \qquad (2.5)$$

These estimates for g_M and g_P come from the conserved vector current (CVC) hypothesis and from the partially conserved axial vector current (PCAC) hypothesis, respectively. In the numerical calculation we will use an effective axial-vector coupling $g_A = 1$ [19–21].

The finite nuclear size (FNS) effect is incorporated via the dipole form factor with a cutoff $\Lambda = 850$ MeV, that is, as

$$g \rightarrow g\left(\frac{\Lambda^2}{\Lambda^2 + k^2}\right)^2.$$

To use (2.1) with nonrelativistic nuclear wave functions, the Foldy-Wouthuysen transformation has to be performed on the hadronic current (2.2). When the velocity-dependent terms are included this yields

$$J_\emptyset = g_V + (\overline{g}_A + \overline{g}_{P1})\boldsymbol{\sigma}\cdot\hat{\mathbf{k}} - g_A\boldsymbol{\sigma}\cdot\mathbf{v},$$
$$\mathbf{J} = -g_A\boldsymbol{\sigma} - i\overline{g}_W\boldsymbol{\sigma}\times\hat{\mathbf{k}} - \overline{g}_V\hat{\mathbf{k}} + \overline{g}_{P2}(\boldsymbol{\sigma}\cdot\hat{\mathbf{k}})\hat{\mathbf{k}} + g_V\mathbf{v},$$
$$(2.6)$$

where $\mathbf{v} \equiv -i\boldsymbol{\nabla}/\text{M}$ is the velocity operator, acting on the nuclear wave functions. The following shorthand notation has been introduced:

$$\overline{g}_V = g_V\frac{\kappa}{2\text{M}}, \qquad \overline{g}_A = g_A\frac{\kappa}{2\text{M}}, \quad \overline{g}_W = (g_V + g_M)\frac{\kappa}{2\text{M}},$$
$$\overline{g}_{P1} = g_P\frac{\kappa}{2\text{M}}\frac{k_\emptyset}{\text{m}_\ell}, \quad \overline{g}_{P2} = g_P\frac{\kappa}{2\text{M}}\frac{\kappa}{\text{m}_\ell}, \qquad (2.7)$$

where $\kappa \equiv |\mathbf{k}|$.

In performing the multipole expansion of the nuclear operator

$$O_\alpha \equiv (\mathbf{O}, iO_\emptyset) = J_\alpha e^{-i\mathbf{k}\cdot\mathbf{r}}, \qquad (2.8)$$

the momentum $\mathbf{k}$ is taken to be along the z axis, that is,

$$e^{-i\mathbf{k}\cdot\mathbf{r}} = \sum_L i^{-L}\sqrt{4\pi(2L+1)}j_L(\kappa r)Y_{L0}(\hat{\mathbf{r}}), \qquad (2.9)$$

and one gets

$$O_\emptyset = \sum_J i^{-J}\sqrt{4\pi(2J+1)}j_J(\kappa r)Y_{J0}(\hat{\mathbf{r}})J_\emptyset,$$
$$O_M = \sum_{JL} i^{-L}F_{JLM}\sqrt{4\pi(2J+1)}j_L(\kappa r)[Y_L(\hat{\mathbf{r}}) \otimes \mathbf{J}]_{JM}.$$
$$(2.10)$$

The geometrical factors

$$F_{JLM} \equiv (-)^{J+M}\sqrt{(2L+1)}\begin{pmatrix} L & 1 & J \\ 0 & -M & M \end{pmatrix}, \qquad (2.11)$$

---

[1]To avoid confusion, we will be using roman fonts (M, m) for masses and math italic fonts (M, m) for azimuthal quantum numbers.

TABLE I. Values of the geometrical factors F_{JLM}.

M	L	F_{JLM}
0	$J+1$	$-\sqrt{\frac{J+1}{2J+1}}$
0	J	0
0	$J-1$	$\sqrt{\frac{J}{2J+1}}$
1	$J+1$	$\frac{1}{\sqrt{2}}\sqrt{\frac{J}{2J+1}}$
1	J	$-\frac{1}{\sqrt{2}}$
1	$J-1$	$\frac{1}{\sqrt{2}}\sqrt{\frac{J+1}{2J+1}}$
-1	$J+1$	$\frac{1}{\sqrt{2}}\sqrt{\frac{J}{2J+1}}$
-1	J	$\frac{1}{\sqrt{2}}$
-1	$J-1$	$\frac{1}{\sqrt{2}}\sqrt{\frac{J+1}{2J+1}}$

which will be seldom used in our work, fulfill the sum rule

$$\sum_L F_{JLM}F_{JLM'} = \delta_{MM'}, \qquad (2.12)$$

and their explicit values are listed in Table I.

After performing some Racah algebra we find

$$O_\alpha = \sum_J \sqrt{2J+1}\, \mathsf{O}_\alpha(J), \qquad (2.13)$$

with

$$\mathsf{O}_\emptyset(J) = i^{-J}\sqrt{4\pi}[g_V\mathsf{Y}_{J0}(\kappa\mathbf{r}) - g_A\mathsf{Y}_{J0}(\kappa\mathbf{r}, \boldsymbol{\sigma}\cdot\mathbf{v})]$$
$$+ \sqrt{4\pi}\left(\overline{g}_A + \overline{g}_{P1}\right)\sum_{L=J\pm 1} i^{-L}F_{JL0}\mathsf{S}_{JL0}(\kappa\mathbf{r}) \qquad (2.14)$$

and

$$\mathsf{O}_M(J) = \sqrt{4\pi}\sum_L i^{-L}F_{JLM}\Big[-g_A\mathsf{S}_{JLM}(\kappa\mathbf{r}) + g_V\mathsf{P}_{JLM}(\kappa\mathbf{r})$$
$$- i(-)^J\overline{g}_V F_{JL0}\mathsf{Y}_{JM}(\kappa\mathbf{r}) + \sum_I (i(-)^L\overline{g}_W G_{JLI}$$
$$+ \overline{g}_{P2}F_{JL0}F_{JI0})\mathsf{S}_{JIM}(\kappa\mathbf{r})\Big], \qquad (2.15)$$

where we have introduced the operators listed in Table II, along with the coefficients

$$G_{JLI} = (-)^J\sqrt{6(2L+1)(2I+1)}\begin{Bmatrix}1 & 1 & 1 \\ I & L & J\end{Bmatrix}\begin{pmatrix}I & 1 & L \\ 0 & 0 & 0\end{pmatrix}, \qquad (2.16)$$

TABLE II. Elemental operators and their parities.

Operator	Parity
$\mathsf{Y}_{JM}(\kappa\mathbf{r}) = j_J(\kappa r)Y_{JM}(\hat{\mathbf{r}})$	$(-)^J$
$\mathsf{S}_{JLM}(\kappa\mathbf{r}) = j_L(\kappa r)[Y_L(\hat{\mathbf{r}})\otimes\boldsymbol{\sigma}]_{JM}$	$(-)^L$
$\mathsf{P}_{JLM}(\kappa\mathbf{r}) = j_L(\kappa r)[Y_L(\hat{\mathbf{r}})\otimes\mathbf{v}]_{JM}$	$(-)^{L+1}$
$\mathsf{Y}_{JM}(\kappa\mathbf{r}, \boldsymbol{\sigma}\cdot\mathbf{v}) = j_J(\kappa r)Y_{JM}(\hat{\mathbf{r}})(\boldsymbol{\sigma}\cdot\mathbf{v})$	$(-)^{J+1}$

which obey the sum rule

$$\sum_L F_{JLM}G_{JLI} = -MF_{JIM}. \qquad (2.17)$$

Using (2.12) and (2.17) we can rewrite the spherical components of $\mathsf{O}_M(J)$ as

$$\mathsf{O}_M(J) = \sqrt{4\pi}\sum_L i^{-L}F_{JLM}[(-g_A + M\overline{g}_W + \overline{g}_{P2}\delta_{M0})$$
$$\times \mathsf{S}_{JLM}(\kappa\mathbf{r}) + g_V\mathsf{P}_{JLM}(\kappa\mathbf{r})]$$
$$- \sqrt{4\pi}i^{-J}\overline{g}_V\delta_{M0}\mathsf{Y}_{J0}(\kappa\mathbf{r}). \qquad (2.18)$$

For the neutrino-nucleus reaction the momentum transfer is $k = p_\ell - q_\nu$, with $p_\ell \equiv \{\mathbf{p}_\ell, iE_\ell\}$ and $q_\nu \equiv \{\mathbf{q}_\nu, iE_\nu\}$, and the corresponding cross section reads

$$\sigma(E_\ell, J_f) = \frac{|\mathbf{p}_\ell|E_\ell}{2\pi}F(Z+1, E_\ell)\int_{-1}^1 d(\cos\theta)\mathcal{T}_\sigma(\kappa, J_f), \qquad (2.19)$$

where $F(Z+1, E_\ell)$ is the Fermi function, $\theta \equiv \hat{\mathbf{q}}_\nu \cdot \hat{\mathbf{p}}_\ell$, and

$$\mathcal{T}_\sigma(\kappa, J_f) \equiv \frac{1}{2J_i+1}\sum_{s_\ell, s_\nu}\sum_{M_i, M_f}|\langle J_f M_f|H_W|J_i M_i\rangle|^2, \qquad (2.20)$$

with $|J_i M_i\rangle$ and $|J_f M_f\rangle$ being the nuclear initial and final state vectors.

The weak Hamiltonian matrix element reads

$$\langle J_f M_f|H_W|J_i M_i\rangle = \frac{G}{\sqrt{2}}\mathcal{O}_\alpha l_\alpha, \qquad (2.21)$$

where

$$\mathcal{O}_\alpha \equiv \langle J_f M_f|O_\alpha|J_i M_i\rangle, \qquad (2.22)$$

and l_α is the leptonic current defined in (2.3). Thus

$$\mathcal{T}_\sigma(\kappa, J_f) = \frac{G^2}{2J_i+1}\sum_{M_iM_f}\mathcal{O}_\alpha\mathcal{O}_\beta^*\mathcal{L}_{\alpha\beta}, \qquad (2.23)$$

where the lepton trace $\mathcal{L}_{\alpha\beta}$, when expressed in Cartesian spatial coordinates, reads

$$\mathcal{L}_{\alpha\beta} = \frac{1}{2}\sum_{s_\ell s_\nu}l_\alpha l_\beta^* = -\frac{1}{E_\ell E_\nu}[p_\alpha q_\beta + q_\alpha p_\beta$$
$$- \delta_{\alpha\beta}(p\cdot q)\pm\epsilon_{\alpha\beta\gamma\delta}q_\gamma p_\delta], \qquad (2.24)$$

with the positive (negative) sign standing for neutrino (antineutrino) scattering.

It is convenient to follow Ref. [15] and express the spatial parts of $\mathcal{O}$ and $\mathcal{L}$ in spherical coordinates ($M, M' = 0, -1, 1$). In this way one might write

$$\mathcal{T}_\sigma(\kappa, J_f) = \frac{G^2}{2J_i+1}\sum_{M_f M_i}\left[|\mathcal{O}_\emptyset|^2\mathcal{L}_{\emptyset\emptyset} + \sum_{MM'}\mathcal{O}_M\mathcal{O}_{M'}^*\mathcal{L}_{MM'}\right.$$
$$\left. - 2\Re\left(\mathcal{O}_\emptyset^*\sum_M(-)^M\mathcal{O}_{-M}\mathcal{L}_{\emptyset M}\right)\right], \qquad (2.25)$$

with [15]

$$\mathcal{L}_{\emptyset\emptyset} \equiv \mathcal{L}_{44} = 1 + \frac{\mathbf{p}\cdot\mathbf{q}}{E_\ell E_\nu}, \qquad (2.26)$$

$$\mathcal{L}_{\emptyset M} \equiv -i\mathcal{L}_{4M} = \frac{1}{E_\ell E_\nu}\left[E_\ell q_M + E_\nu p_M \mp i(\mathbf{q} \times \mathbf{p})_M\right],$$
(2.27)

$$\mathcal{L}_{MM'} = \delta_{MM'} + \frac{1}{E_\ell E_\nu}(q_M^* p_{M'} + q_{M'} p_M^* - \delta_{MM'}\mathbf{p}\cdot\mathbf{q})$$
$$\pm \sqrt{6}(-)^M \begin{pmatrix} 1 & 1 & 1 \\ -M & M' & M-M' \end{pmatrix}\left(\frac{q_{M-M'}^*}{E_\nu} - \frac{p_{M-M'}^*}{E_\ell}\right).$$
(2.28)

From the Wigner-Eckart theorem we also get

$$\mathcal{O}_\emptyset = \sum_J (-)^{J_f - M_f}\sqrt{2J+1} \begin{pmatrix} J_f & J & J_i \\ -M_f & 0 & M_i \end{pmatrix}\langle J_f\|\mathsf{O}_\emptyset(J)\|J_i\rangle$$
(2.29)

and

$$\mathcal{O}_M = \sum_J (-)^{J_f - M_f}\sqrt{2J+1} \begin{pmatrix} J_f & J & J_i \\ -M_f & M & M_i \end{pmatrix}$$
$$\times \langle J_f\|\mathsf{O}_M(J)\|J_i\rangle.$$
(2.30)

Using the orthogonality condition

$$\sum_{M_i M_f} \begin{pmatrix} J_f & J & J_i \\ -M_f & M & M_i \end{pmatrix}\begin{pmatrix} J_f & J' & J_i \\ -M_f & M' & M_i \end{pmatrix} = \frac{1}{(2J+1)}\delta_{JJ'}\delta_{MM'}$$
(2.31)

one obtains

$$\mathcal{T}_\sigma(\kappa, J_f) = \frac{G^2}{2J_i+1}\sum_J \Bigg[|\langle J_f\|\mathsf{O}_\emptyset(J)\|J_i\rangle|^2\mathcal{L}_{\emptyset\emptyset}$$
$$+ \sum_M |\langle J_f\|\mathsf{O}_M(J)\|J_i\rangle|^2\mathcal{L}_{MM}$$
$$- 2\Re(\langle J_f\|\mathsf{O}_\emptyset(J)\|J_i\rangle^*\langle J_f\|\mathsf{O}_0(J)\|J_i\rangle\mathcal{L}_{\emptyset 0})\Bigg],$$
(2.32)

where, from (2.14) and (2.18),

$$\langle J_f\|\mathsf{O}_\emptyset(J)\|J_i\rangle = \sqrt{2J_i+1}[g_V\mathcal{M}_V(J) - g_A\mathcal{M}_{A'}(J)$$
$$+ (\overline{g}_A + \overline{g}_{P1})\mathcal{M}_A^0(J)]$$
$$\langle J_f\|\mathsf{O}_M(J)\|J_i\rangle = \sqrt{2J_i+1}\big[(-g_A + M\overline{g}_W + \overline{g}_{P2}\delta_{M0})$$
$$\times \mathcal{M}_A^M(J) + g_V\mathcal{M}_{V'}^M(J)$$
$$- \overline{g}_V\delta_{M0}\mathcal{M}_V(J)\big],$$
(2.33)

with the nuclear matrix elements defined as

$$\mathcal{M}_V(J) = i^{-J}\sqrt{\frac{4\pi}{2J_i+1}}\langle J_f\|\mathsf{Y}_J(\kappa\mathbf{r})\|J_i\rangle,$$

$$\mathcal{M}_A^M(J) = \sqrt{\frac{4\pi}{2J_i+1}}\sum_L i^{-L}F_{JLM}\langle J_f\|\mathsf{S}_{JL}(\kappa\mathbf{r})\|J_i\rangle,$$
(2.34)

$$\mathcal{M}_{A'}(J) = i^{-J}\sqrt{\frac{4\pi}{2J_i+1}}\langle J_f\|\mathsf{Y}_J(\kappa\mathbf{r}, \boldsymbol{\sigma}\cdot\mathbf{v})\|J_i\rangle,$$

$$\mathcal{M}_{V'}^M(J) = \sqrt{\frac{4\pi}{2J_i+1}}\sum_L i^{-L}F_{JLM}\langle J_f\|\mathsf{P}_{JL}(\kappa\mathbf{r})\|J_i\rangle.$$

The explicit expressions for $\mathcal{L}_{\emptyset M}$ and $\mathcal{L}_{MM'}$ that appear in (2.32) are [14]

$$\mathcal{L}_{\emptyset 0} = \left(\frac{q_0}{E_\nu} + \frac{p_0}{E_\ell}\right),$$
$$\mathcal{L}_{00} = 1 + \frac{2q_0 p_0 - \mathbf{p}\cdot\mathbf{q}}{E_\ell E_\nu},$$
$$\mathcal{L}_{\pm1,\pm1} = 1 - \frac{q_0 p_0}{E_\ell E_\nu} \pm \left(\frac{q_0}{E_\nu} - \frac{p_0}{E_\ell}\right),$$
(2.35)

with

$$q_0 = \hat{\kappa}\cdot\mathbf{q} = \frac{E_\nu(|\mathbf{p}|\cos\theta - E_\nu)}{\kappa},$$
$$p_0 = \hat{\kappa}\cdot\mathbf{p} = \frac{|\mathbf{p}|(|\mathbf{p}| - E_\nu\cos\theta)}{\kappa}.$$
(2.36)

Finally, the transition amplitude can be cast in the form

$$\mathcal{T}_\sigma(\kappa, J_f)$$
$$= G^2\sum_J \Bigg\{\mathcal{L}_{\emptyset\emptyset}\big[g_V^2|\mathcal{M}_V(J)|^2 + \big|(\overline{g}_A + \overline{g}_{P1})\mathcal{M}_A^0(J)$$
$$- g_A\mathcal{M}_{A'}(J)\big|^2\big] + \mathcal{L}_{00}\big[\Re\big[(\overline{g}_V\mathcal{M}_V(J) - 2g_V\mathcal{M}_{V'}^0(J))$$
$$\times \overline{g}_V\mathcal{M}_V^*(J)\big] + \big(\overline{g}_{P2}^2 - 2g_A\overline{g}_{P2}\big)\big|\mathcal{M}_A^0(J)\big|^2\big]$$
$$+ \sum_{M=0,\pm1}\mathcal{L}_{MM}\big|(g_A - M\overline{g}_W)\mathcal{M}_A^M(J) - g_V\mathcal{M}_{V'}^M(J)\big|^2$$
$$+ 2\mathcal{L}_{\emptyset 0}\Re\big(g_V\big[\,\overline{g}_V\mathcal{M}_V(J) - g_V\mathcal{M}_{V'}^0(J)\big]\mathcal{M}_V^*(J)$$
$$+ (g_A - \overline{g}_{P2})\big[(\overline{g}_A + \overline{g}_{P1})\mathcal{M}_A^0(J)$$
$$- g_A\mathcal{M}_{A'}(J)\,\big]\mathcal{M}_A^{0*}(J)\big)\Bigg\}.$$
(2.37)

The muon-capture transition amplitude $\mathcal{T}_\Lambda(J_f)$ can be derived from the result (2.32) for the neutrino-nucleus reaction amplitude, by keeping in mind that (i) the roles of p and q are interchanged within the matrix element of the leptonic current, which brings in a minus sign in the last term of $\mathcal{L}_{\pm1,=1}$, (ii) the momentum transfer turns out to be $k = q - p$, and therefore the signs of the right-hand sides of (2.36) have to be changed, and (iii) the threshold values ($\mathbf{p} \to 0 : k \to \mathbf{q}, k_\emptyset \to E_\nu - \mathrm{m}_\ell$) must be used for the lepton traces. All this yields

$$\mathcal{L}_{\emptyset\emptyset} = \mathcal{L}_{00} = \mathcal{L}_{\emptyset 0} = 1, \mathcal{L}_{\pm1,\pm1} = 1 \mp 1.$$
(2.38)

One should also remember that instead of summing over the initial lepton spins s_ℓ, as done in (2.20), one now has to average over the same quantum number, getting

$$\Lambda(J_f) = \frac{E_\nu^2}{2\pi}|\phi_{1S}|^2\mathcal{T}_\Lambda(J_f),$$
(2.39)

where ϕ_{1S} is the muonic bound state wave function evaluated at the origin, and $E_\nu = \mathrm{m}_\mu - (M_n - M_p) - E_B^\mu - E_f + E_i,$

where E_B^μ is the binding energy of the muon in the $1S$ orbit. In view of (2.39) the transition amplitude reads

$$\mathcal{T}_\Lambda(J_f) = \frac{G^2}{2J_i + 1} \sum_J [|\langle J_f \| \mathsf{O}_\emptyset(J) - \mathsf{O}_0(J) \| J_i\rangle|^2$$
$$+ 2|\langle J_f \| \mathsf{O}_{-1}(J) \| J_i\rangle|^2], \qquad (2.40)$$

which, based on parity considerations, can be expressed as

$$\mathcal{T}_\Lambda(J_f) = G^2 \sum_J \left\{ \left|(g_V + \overline{g}_V)\mathcal{M}_V(J) - g_V\mathcal{M}_{V'}^0(J)\right|^2 \right.$$
$$+ \left|(g_A + \overline{g}_A - \overline{g}_P)\mathcal{M}_A^0(J) - g_A\mathcal{M}_{A'}(J)\right|^2$$
$$\left. + 2\left|(g_A + \overline{g}_W)\mathcal{M}_A^{-1}(J) - g_V\mathcal{M}_{V'}^{-1}(J)\right|^2 \right\}, \qquad (2.41)$$

where $\overline{g}_P = \overline{g}_{P2} - \overline{g}_{P1}$. In the case of muon capture, it is convenient to rewrite the effective coupling constants as [11]

$$\overline{g}_V = g_V \frac{E_\nu}{2M}, \quad \overline{g}_A = g_A \frac{E_\nu}{2M},$$
$$\overline{g}_W = (g_V + g_M) \frac{E_\nu}{2M}, \quad \overline{g}_{P1} = g_P \frac{E_\nu}{2M}. \qquad (2.42)$$

Lastly, we mention that the B-values for the Gamow-Teller (GT) β transitions, are defined and related to the ft-values as [22]

$$\frac{|g_A\langle J_f \| \sigma \| J_i\rangle|^2}{2J_i + 1} \equiv B(\text{GT}) = \frac{6146}{ft} \text{ sec.} \qquad (2.43)$$

Let us now compare our matrix elements with those currently used in the literature. First, in Walecka's notation (see Eqs. (45.13) in Ref. [7]) one has

$$\mathsf{O}_\emptyset(J) = \mathcal{M}_{J0},$$
$$\mathsf{O}_M(J) = \begin{cases} \mathcal{L}_{J0}, & \text{for } M = 0, \\ -\frac{1}{\sqrt{2}}\left[M\mathcal{T}_{JM}^{\text{mag}} + \mathcal{T}_{JM}^{\text{el}}\right], & \text{for } M = \pm 1, \end{cases} \qquad (2.44)$$

where the meaning of $\mathcal{M}_{J0}$ and $\mathcal{L}_{J0}$ is self-evident, and

$$\mathcal{T}_{JM}^{\text{el}} = \overline{g}_W \mathsf{S}_{JJM} - i^J \sqrt{2} \sum_{L=J\pm 1} i^{-L} F_{JLM}$$
$$\times [g_A \mathsf{S}_{JLM} - g_V \mathsf{P}_{JLM}],$$
$$\mathcal{T}_{JM}^{\text{mag}} = -g_A \mathsf{S}_{JJM} + g_V \mathsf{P}_{JJM} + i^J \sqrt{2}\overline{g}_W$$
$$\times \sum_{L=J\pm 1} i^{-L} F_{JLM} \mathsf{S}_{JLM}. \qquad (2.45)$$

The matrix elements defined by Donelly [6] are related to ours as

$$M_J^M(\kappa\mathbf{r}) = \mathsf{Y}_{JM}(\kappa\mathbf{r}),$$
$$\Delta_J^M(\kappa\mathbf{r}) = \left(\frac{i\mathsf{M}}{\kappa}\right) \mathsf{P}_{JJM}(\kappa\mathbf{r}),$$
$$\Delta_J'^M(\kappa\mathbf{r}) = i^J \sqrt{2} \left(\frac{\mathsf{M}}{\kappa}\right) \sum_{L=J\pm 1} i^{-L} F_{JLM} \mathsf{P}_{LJM}(\kappa\mathbf{r}),$$
$$\Sigma_J^M(\kappa\mathbf{r}) = \mathsf{S}_{JJM}(\kappa\mathbf{r}), \qquad (2.46)$$

$$\Sigma_J'^M(\kappa\mathbf{r}) = i^{J-1}\sqrt{2} \sum_{L=J\pm 1} i^{-L} F_{JLM} \mathsf{S}_{JLM}(\kappa\mathbf{r}),$$
$$\Sigma_J''^M(\kappa\mathbf{r}) = i^{J-1} \sum_{L=J\pm 1} i^{-L} F_{JL0} \mathsf{S}_{JLM}(\kappa\mathbf{r}),$$
$$\Omega_J^M(\kappa\mathbf{r}) = \left(\frac{i\mathsf{M}}{\kappa}\right) \mathsf{Y}_{JM}(\kappa\mathbf{r}, \boldsymbol{\sigma} \cdot \mathbf{v}).$$

The relationship between our formalism and those from Refs. [10,11] can be obtained from the formula

$$\begin{pmatrix} L & 1 & J \\ 0 & M & -M \end{pmatrix} \begin{pmatrix} L' & 1 & J \\ 0 & M & -M \end{pmatrix}$$
$$= \frac{\delta_{LL'}}{3(2L+1)} - M\sqrt{\frac{3}{2}} \begin{pmatrix} L & L' & 1 \\ 0 & 0 & 0 \end{pmatrix} \begin{Bmatrix} L & 1 & J \\ 1 & L' & 1 \end{Bmatrix}$$
$$+ (-)^{J+1} \sqrt{\frac{5}{6}}(3M^2 - 2) \begin{pmatrix} L & L' & 2 \\ 0 & 0 & 0 \end{pmatrix} \begin{Bmatrix} L & 1 & J \\ 1 & L' & 2 \end{Bmatrix}. \qquad (2.47)$$

For the matrix elements of Kuramoto *et al.* [10] we get

$$|\langle f|\tilde{1}|i\rangle|^2 = \sum_J |\mathcal{M}_V(J)|^2,$$
$$\langle f|\tilde{\sigma}|i\rangle|^2 = \sum_J \sum_{M=0,\pm 1} \left|\mathcal{M}_A^M(J)\right|^2,$$
$$\Lambda = \frac{1}{3} \sum_J \left(\left|\mathcal{M}_A^0(J)\right|^2 - \left|\mathcal{M}_A^1(J)\right|^2\right); \qquad (2.48)$$

and for those of Luyten *et al.* [11] we get

$$M_V^2 = \left(\frac{E_\nu}{m_\mu}\right)^2 \sum_J |\mathcal{M}_V(J)|^2,$$
$$M_A^2 = \left(\frac{E_\nu}{m_\mu}\right)^2 \sum_J \sum_{M=0,\pm 1} \left|\mathcal{M}_A^M(J)\right|^2, \qquad (2.49)$$
$$M_P^2 = \left(\frac{E_\nu}{m_\mu}\right)^2 \sum_J \left|\mathcal{M}_A^0(J)\right|^2.$$

III. PQRPA FORMALISM

We have shown in Ref. [14] that to account for the weak decay observables in a light $N = Z$ nucleus in the framework of the RPA, besides including the BCS correlations, it is imperative to perform the particle number projection. It should be remembered that in heavy nuclei the neutron excess is usually large, which makes the projection procedure less important than in light nuclei [23]. In this section we give a more detailed overview of the PBCS and approximation PQRPA.

When the excited states $|J_f\rangle$ in the final $(Z \pm 1, N \mp 1)$ nuclei are described within the PQRPA, the transition amplitudes for the multipole charge-exchange operators Y_J, etc. listed in Table II read

$$\langle J_f, Z + \mu, N - \mu \| \mathsf{Y}_J \| 0^+\rangle$$
$$= \frac{1}{(I^Z I^N)^{1/2}} \sum_{pn} \left[\frac{\Lambda_\mu(pnJ)}{(I^{Z-1+\mu}(p)I^{N-1+\mu}(n))^{1/2}} X_\mu^*(pnJ_f) \right.$$
$$\left. + \frac{\Lambda_{-\mu}(pnJ)}{(I^{Z-1-\mu}(p)I^{N-1-\mu}(n))^{1/2}} Y_\mu^*(pnJ_f) \right], \qquad (3.1)$$

with the one-body matrix elements given by

$$\Lambda_\mu(pnJ) = -\frac{\langle p\|\mathsf{Y}_J\|n\rangle}{\sqrt{2J+1}}\begin{cases} u_p v_n, & \text{for } \mu = +1, \\ u_n v_p, & \text{for } \mu = -1, \end{cases} \quad (3.2)$$

where

$$I^K(k_1 k_2 \cdots k_n) = \frac{1}{2\pi i}\oint \frac{dz}{z^{K+1}}\sigma_{k_1}\cdots\sigma_{k_n}\prod_k (u_k^2 + z^2 v_k^2)^{j_k+1/2},$$

$$\sigma_k^{-1} = u_k^2 + z_k^2 v_k^2, \quad (3.3)$$

are the PBCS number projection integrals.

The PBCS gap equations are

$$2\bar{e}_k u_k v_k - \Delta_k(u_k^2 - v_k^2) = 0, \quad (3.4)$$

where

$$\Delta_k = -\frac{1}{2}\sum_{k'}\frac{(2j_{k'}+1)^{1/2}}{(2j_k+1)^{1/2}}u_{k'}v_{k'}\mathrm{G}(kkk'k';0)\frac{I^{Z-2}(kk')}{I^Z} \quad (3.5)$$

are the pairing gaps, and

$$\bar{e}_k = e_k \frac{I^{Z-2}(k)}{I^Z} + \sum_{k'}\frac{(2j_{k'}+1)^{1/2}}{(2j_k+1)^{1/2}}v_{k'}^2$$
$$\times \mathrm{F}(kkk'k';0)\frac{I^{Z-4}(kk')}{I^Z} + \Delta e_k \quad (3.6)$$

are the dressed single-particle energies. The PBCS correction term Δe_k can be found in Ref. [23], and F and G stand for the usual particle-hole (ph) and particle-particle (pp) matrix elements, respectively.

The forward, X_μ, and backward, Y_μ, PQRPA amplitudes are obtained by solving the RPA equations

$$\begin{pmatrix} A_\mu & B \\ -B^* & -A_{-\mu}^* \end{pmatrix}\begin{pmatrix} X_\mu \\ Y_\mu \end{pmatrix} = \omega_\mu\begin{pmatrix} X_\mu \\ Y_\mu \end{pmatrix}, \quad (3.7)$$

with the PQRPA matrices defined as

$$A_\mu(pn, p'n'; J)$$
$$= (\varepsilon_p^{Z-1+\mu} + \varepsilon_n^{N-1-\mu})\delta_{pn,p'n'} + N_\mu(pn)^{-1/2}N_\mu(p'n')^{-1/2}$$
$$\times \{[u_p v_n u_{p'} v_{n'} I^{Z-1+\mu}(pp') I^{N-3-\mu}(nn')$$
$$+ v_p u_n v_{p'} u_{n'} I^{Z-3+\mu}(pp') I^{N-1-\mu}(nn')]\mathrm{F}(pn, p'n'; J)$$
$$+ [u_p u_n u_{p'} u_{n'} I^{Z-1+\mu}(pp') I^{N-1-\mu}(nn')$$
$$+ v_p v_n v_{p'} v_{n'} I^{Z-3+\mu}(pp') I^{N-3-\mu}(nn')]\mathrm{G}(pn, p'n'; J)\},$$
$$B(pn, p'n'; J)$$
$$= N_\mu(pn)^{-1/2}N_{-\mu}(p'n')^{-1/2}I^{Z-2}(pp') I^{N-2}(nn')$$
$$\times [(v_p u_n u_{p'} v_{n'} + u_p v_n v_{p'} u_{n'})\mathrm{F}(pn, p'n'; J)$$
$$+ (u_p u_n v_{p'} v_{n'} + v_p v_n u_{p'} u_{n'})\mathrm{G}(pn, p'n'; J)], \quad (3.8)$$

where

$$N_\mu(pn) = I^{Z-1+\mu}(p) I^{N-1-\mu}(n) \quad (3.9)$$

are the norms,

$$\varepsilon_k^K = \frac{R_0^K(k) + R_{11}^K(kk)}{I^K(k)} - \frac{R_0^K}{I^K} \quad (3.10)$$

are the projected quasiparticle energies, and the quantities R^K are defined as [23]

$$R_0^K(k) = \sum_{k_1}(2j_{k_1}+1)v_{k_1}^2 e_{k_1} I^{K-2}(kk_1)$$
$$+ \frac{1}{4}\sum_{k_1 k_2}(2j_{k_1}+1)^{1/2}(2j_{k_2}+1)^{1/2}$$
$$\times [v_{k_1}^2 v_{k_2}^2 \mathrm{F}(k_1 k_1 k_2 k_2; 0) I^{K-4}(k_1 k_2 k)$$
$$+ u_{k_1}v_{k_1}u_{k_2}v_{k_2}\mathrm{G}(k_1 k_1 k_2 k_2; 0) I^{K-2}(k_1 k_2 k)],$$

$$R_{11}^K(kk) = e_k[u_k^2 I^{k_1}(kk) - v_k^2 I^{K-2}(kk)] + \sum_{k_1}\frac{(2j_{k_1}+1)^{1/2}}{(2j_k+1)^{1/2}}$$
$$\times \{v_{k_1}^2 \mathrm{F}(k_1 k_1 kk; 0)[u_k^2 I^{K-2}(k_1 kk) - v_k^2 I^{K-4}(k_1 kk)]$$
$$- u_{k_1}v_{k_1}u_k v_k \mathrm{G}(k_1 k_1 kk; 0) I^{K-2}(k_1 kk)\}. \quad (3.11)$$

It is worth noting that the PQRPA formalism is valid not only for the particle-hole charge-exchange excitations ($Z \pm 1$, $N \mp 1$) but also for the charge-exchange pairing vibrations ($Z \pm 1$, $N \pm 1$). In the later case one simply has to make the replacement $\mu \to -\mu$ in the neutron sector.

The usual gap equations are obtained from Eqs. (3.4)–(3.6) by doing the following:

1. Make the replacement $e_k \to e_k - \lambda_k$, with λ_k being the chemical potential, and taking the limit $I^K \to 1$. That is, Eq. (3.4) remains as it is, but instead of (3.5) and (3.6) one now has

$$\Delta_k = -\frac{1}{2}\sum_{k'}\frac{(2j_{k'}+1)^{1/2}}{(2j_k+1)^{1/2}}u_{k'}v_{k'}\mathrm{G}(kkk'k';0) \quad (3.12)$$

and

$$\bar{e}_k = e_k - \lambda_k + \sum_{k'}\frac{(2j_{k'}+1)^{1/2}}{(2j_k+1)^{1/2}}v_{k'}^2\mathrm{F}(kkk'k';0). \quad (3.13)$$

2. Impose the subsidiary conditions

$$Z = \sum_{j_p}(2j_p+1)^2 v_{j_p}^2, \quad N = \sum_{j_n}(2j_n+1)^2 v_{j_n}^2, \quad (3.14)$$

as the number of particles is no longer a good quantum number.

Finally, the plain QRPA equations are recovered from (3.7) and (3.8) by (i) dropping the index μ and taking the limit $I^K \to 1$ and (ii) substituting the unperturbed PBCS energies by the BCS energies relative to the Fermi level, that is, by

$$E_k^{(\pm)} = \pm E_k + \lambda_k, \quad (3.15)$$

where $E_k = (\bar{e}_k^2 + \Delta_k^2)^{1/2}$ are the usual BCS quasiparticle energies. In this way the unperturbed energies in (3.8) are replaced as[2]

$$\varepsilon_{j_p}^{Z-1+\mu} + \varepsilon_{j_n}^{N-1-\mu} \to E_{j_p} + E_{j_n} + \mu(\lambda_p - \lambda_n). \quad (3.16)$$

---

[2]We note that there are misprints in [14, (23)].

TABLE III. BCS and PBCS results for neutrons. E_j^{exp} stands for the experimental energies used in the fitting procedure, and e_j are the resulting single-particle energies. The underlined quasiparticle energies correspond to single-hole excitations (for $j_h = 1s_{1/2}, 1p_{3/2}$) and to single-particle excitations (for $j_p = 1p_{1/2}, 1d_{5/2}, 2s_{1/2}, 1d_{3/2}, 1f_{7/2}, 2p_{3/2}, 2p_{1/2}, 1f_{5/2}$). The nonunderlined energies are mostly two-hole/one-particle and two-particle/one-hole excitations. The fitted values of the pairing strengths v_s^{pair} in units of MeV fm^3 are also displayed.

Shell	E_j^{exp}	BCS			PBCS		
		$E_j^{(+)}$	$E_j^{(-)}$	e_j	ε_j^N	$-\varepsilon_j^{N-2}$	e_j
$1s_{1/2}$		11.34	-35.13	-23.58	19.93	-34.99	-22.37
$1p_{3/2}$	-18.72	-5.07	$\underline{-18.72}$	-7.80	-1.28	$\underline{-18.73}$	-7.24
$1p_{1/2}$	-4.94	$\underline{-4.94}$	-18.85	-2.07	$\underline{-4.95}$	-22.33	-1.51
$1d_{5/2}$	-1.09	$\underline{-1.09}$	-22.70	2.12	$\underline{-1.09}$	-26.82	2.16
$2s_{1/2}$	-1.85	$\underline{-1.86}$	-21.93	2.70	$\underline{-1.85}$	-25.98	2.68
$1d_{3/2}$	2.72	$\underline{2.72}$	-26.51	6.24	$\underline{2.73}$	-30.79	6.26
$1f_{7/2}$	5.81	$\underline{5.82}$	-29.61	8.14	$\underline{5.83}$	-33.61	8.17
$2p_{3/2}$	7.17	$\underline{7.18}$	-30.98	11.49	$\underline{7.16}$	-35.23	11.47
$2p_{1/2}$		$\underline{12.89}$	-36.69	17.30	$\underline{12.89}$	-41.01	17.32
$1f_{5/2}$		$\underline{16.72}$	-40.52	19.18	$\underline{16.72}$	-44.58	19.21
v_s^{pair}				23.16			23.92

IV. NUMERICAL RESULTS AND DISCUSSION

In this section, our theoretical results within the PQRPA are confronted with the experimental data for the $\mu^- +^{12}\mathrm{B} \to {}^{12}\mathrm{C} + \nu_\mu$ muon-capture rates, as well as for the neutrino cross sections involving the DAR reaction $\nu_e +^{12}\mathrm{C} \to {}^{12}\mathrm{N} + e^-$ and DIF reaction $\nu_\mu + {}^{12}\mathrm{C} \to {}^{12}\mathrm{N} + \mu^-$. We also make our predictions for the $\nu_e + {}^{12}\mathrm{C} \to {}^{12}\mathrm{N} + e^-$ differential cross section for ν_e energies in the DIF energy range. At variance with our previous work, we consider here also the velocity-dependent matrix elements $\mathcal{M}_{A'}(J)$ and $\mathcal{M}_{V'}^M(J)$, defined in (2.34).

The calculations shown here were done in the same way as in the previous work [14]. That is, for the residual interaction we adopted the delta force,

$$V = -4\pi \left(v_s P_s + v_t P_t\right)\delta(r), \qquad (4.1)$$

which has been used extensively in the literature [24–26] for describing single and double β decays. The configuration space includes the single-particle orbitals with $nl = (1s, 1p, 1d, 2s, 1f, 2p)$ for both protons and neutrons.

Most of the bare single-particle energies e_j, as well as the value of the singlet strength within the pairing channel (v_s^{pair}), were fixed from the experimental energies E_j^{exp} of the odd-mass nuclei ${}^{11}\mathrm{C},{}^{11}\mathrm{B},{}^{13}\mathrm{C}$, and ${}^{13}\mathrm{N}$. That is, in the BCS case, (1) we assume that the ground states in ${}^{11}\mathrm{C}$ and ${}^{11}\mathrm{B}$ are pure quasi-hole excitations $E_{j_h}^{(-)}$, with $j_h = 1p_{3/2}$, and that the lowest observed $1/2^-, 5/2^+, 1/2^+, 3/2^+, 7/2^-$, and $3/2^-$ states in ${}^{13}\mathrm{C}$ and ${}^{13}\mathrm{N}$ are pure quasiparticle excitations $E_{j_p}^{(+)}$ with $j_p = 1p_{1/2}, 1d_{5/2}, 2s_{1/2}, 1d_{3/2}, 1f_{7/2}, 2p_{3/2}$, and (2) the single-particle energies of these seven states and the pairing strength, which appear in the BCS gap equation (3.4), (3.12)–(3.14), are then varied in a χ^2 search to account for the experimental spectra E_j^{exp} [27]. In the PBCS case we proceed in the same way, that is, we solve Eqs. (3.4)–(3.6), and, instead of fitting $E_{j_p}^{(+)}$ and $E_{j_h}^{(-)}$ to E_j^{exp}, we fit

now $\varepsilon_{j_p}^{Z,N}$ and $-\varepsilon_{j_h}^{Z-2,N-2}$. We have considered the faraway orbitals $1s_{1/2}, 2p_{1/2}$, and $1f_{5/2}$ as well, assuming the first one to be a pure hole state and the other two pure particle states. Their single-particle energies were taken to be that of a harmonic oscillator (HO) with standard parametrization [28]. The single-particle wave functions were also approximated with that of the HO with the length parameter $b = 1.67$ fm, which corresponds to the estimate $\hbar\omega = 45A^{-1/3} - 25A^{-2/3}$ MeV for the oscillator energy. The final results for neutrons are shown in Table III and those for protons in Table IV. It is worth noting that the PBCS neutron energy $\varepsilon_{1p_{3/2}}^N = -1.28$ MeV nicely agrees with the experimental energy $E_{3/2_1^-} = -1.26$ MeV in ${}^{13}\mathrm{C}$. In the same way the PBCS proton energy $\varepsilon_{1p_{3/2}}^Z = 1.46$ MeV agrees with the measured energy $E_{3/2_1^-} = 1.55$ MeV in ${}^{13}\mathrm{N}$ [27]. This does not happen in the BCS case, where $E_{1p_{3/2}}^{(+)} = -5.07$ MeV for neutrons and $E_{1p_{3/2}}^{(+)} = -2.44$ MeV for protons, which clearly shows the necessity for the number projection procedure. At this point it could be useful to remember that, although in ${}^{11}\mathrm{C}$ and ${}^{11}\mathrm{B}$ the state $3/2_1^-$ is dominantly a hole state, in ${}^{13}\mathrm{C}$ and ${}^{13}\mathrm{N}$ it is basically a two-particle one-hole state.

Before proceeding let us remember an important issue in the description of the $N \cong Z$ nuclei within the QRPA, which is more inherent to the model itself than to the occasional parametrization that might be employed. In fact, a few years ago Volpe et al. [9] called attention to the inconvenience of applying QRPA to ${}^{12}\mathrm{N}$, since the lowest state turned out not to be the most collective one. Later on we showed [14] that the origin of this difficulty was the degeneracy among the four lowest proton-neutron two-quasiparticle states, $|1p_{1/2}1p_{3/2}\rangle$, $|1p_{3/2}1p_{3/2}\rangle$, $|1p_{1/2}1p_{1/2}\rangle$, and $|1p_{3/2}1p_{1/2}\rangle$. It also has been shown in Ref. [14] that it is imperative to use the PQRPA for a physically sound description of the weak processes among the ground states of the triad $\{{}^{12}\mathrm{B}, {}^{12}\mathrm{C}, {}^{12}\mathrm{N}\}$. In fact, when the Fermi level is fixed at $N = Z = 6$, their BCS

TABLE IV. Same as Table III but for protons.

Shell	E_j^{exp}	BCS			PBCS		
		$E_j^{(+)}$	$E_j^{(-)}$	e_j	ε_j^Z	$-\varepsilon_j^{Z-2}$	e_j
$1s_{1/2}$		14.94	-33.13	-21.62	19.44	-32.99	-20.41
$1p_{3/2}$	-15.95	-2.24	-15.96	-4.95	1.46	-15.95	-4.40
$1p_{1/2}$	-1.94	-1.95	-16.25	1.01	-1.95	-19.76	1.56
$1d_{5/2}$	1.61	1.61	-19.80	4.76	1.61	-23.90	4.83
$2s_{1/2}$	0.42	0.42	-18.61	4.88	0.42	-22.59	4.88
$1d_{3/2}$	4.95	4.95	-23.14	8.40	4.95	-27.37	8.43
$1f_{7/2}$	8.42	8.42	-26.61	10.72	8.42	-30.58	10.75
$2p_{3/2}$	9.76	9.77	-27.96	14.05	9.77	-32.22	14.07
$2p_{1/2}$		16.23	-34.43	20.63	16.22	-38.73	20.66
$1f_{5/2}$		19.70	-37.90	22.15	19.71	-41.96	22.20
v_s^{pair}				23.13			23.92

energies,

$$
\mathcal{E}_{j_p j_n} = \begin{cases} E_{j_p}^{(+)} - E_{j_n}^{(-)} = E_{j_p} + E_{j_n} + \lambda_p - \lambda_n & \text{for } {}^{12}\text{N}, \\ -E_{j_p}^{(-)} + E_{j_n}^{(+)} = E_{j_p} + E_{j_n} - \lambda_p + \lambda_n & \text{for } {}^{12}\text{B}, \\ E_{j_p}^{(+)} + E_{j_n}^{(+)} = E_{j_p} + E_{j_n} + \lambda_p + \lambda_n & \text{for } {}^{14}\text{N}, \\ -E_{j_p}^{(-)} - E_{j_n}^{(-)} = E_{j_p} + E_{j_n} - \lambda_p - \lambda_n & \text{for } {}^{10}\text{B}, \end{cases}
$$
(4.2)

are almost degenerate for all four odd-odd $(Z \pm 1, N \mp 1)$ and $(Z \pm 1, N \pm 1)$ nuclei. As illustrated in Fig. 1, this, in turn, comes from the fact that for $N = Z = 6$ the quasiparticle energies $E_{1p_{1/2}}$ and $E_{1p_{3/2}}$ are very close to each other. The upper panel of Fig. 2 shows the BCS energies (4.2), as a function of N, of these four states for nitrogen isotopes. One notices that for $N \neq Z$ the degeneracy is removed yet only partially. However, as seen from the lower panel in Fig. 2, the degeneracy discussed here is totally removed when the number projection is done.

Moreover, within the PBCS in the case of ^{12}N, for instance, we get from numerical calculations

$$
\begin{aligned} \mathcal{E}_{1p_{3/2}1p_{3/2}} &\cong \mathcal{E}_{1p_{1/2}1p_{1/2}} \cong \mathcal{E}_{1p_{1/2}1p_{3/2}} + \Delta, \\ \mathcal{E}_{1p_{3/2}1p_{1/2}} &\cong \mathcal{E}_{1p_{1/2}1p_{3/2}} + 2\Delta, \end{aligned}
$$
(4.3)

with $\Delta = 3.4$ MeV. The meaning of this results can be easily disentangled by referring to the SM and analyzing the particle-hole (ph) limits of the proton-neutron two-quasiparticle states, which are pictorially shown in Fig. 3. One sees that, whereas $|1p_{1/2}1p_{3/2}\rangle$ corresponds to a 1p1h state in ^{12}N, $|1p_{3/2}1p_{3/2}\rangle$ and $|1p_{1/2}1p_{1/2}\rangle$ correspond to 2p2h states, and $|1p_{3/2}1p_{1/2}\rangle$ to a 3p3h state in the same nucleus. Therefore one can expect that the energy ordering of these states would be given by (4.3), with $\Delta = \Delta_{ls} - \Delta_{pair}$ being the energy difference between the spin-orbit splitting, Δ_{ls}, and the pairing energy, Δ_{pair}. A similar discussion is pertinent to the remaining three nuclei ^{10}B, ^{14}N, and ^{12}B. That is, one expects that their lowest states would be, respectively, $|1p_{3/2}1p_{3/2}\rangle$, $|1p_{1/2}1p_{1/2}\rangle$, and $|1p_{3/2}1p_{1/2}\rangle$, as happens in the PBCS case but not within the BCS. Finally, it is worthwhile to indicate that the same pn quasiparticle excitation

has quite different ph compositions in different nuclei. This can be observed by scrutinizing the four columns in Fig. 3.

The improvement introduced by the PBCS can also be visualized by making a direct calculation of the unperturbed
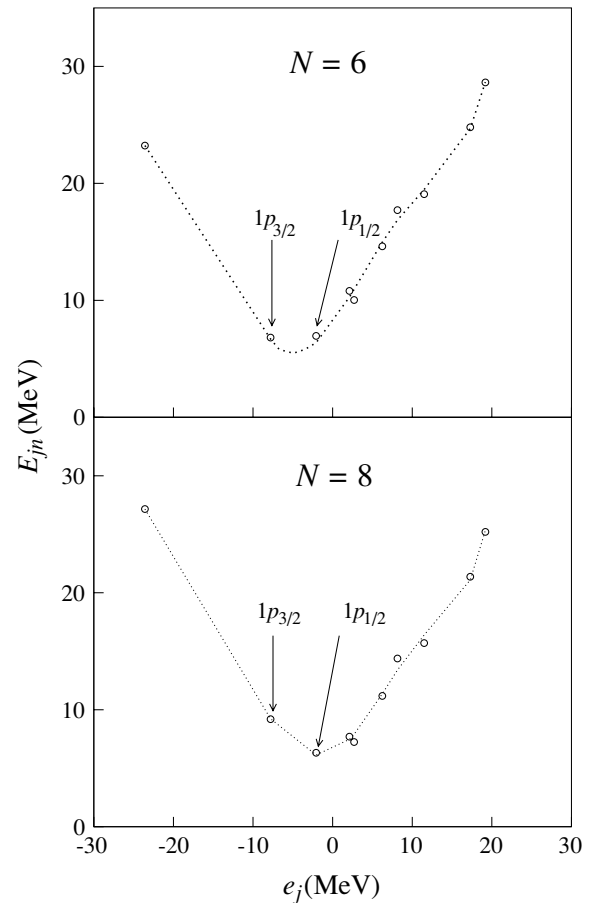

FIG. 1. Neutron quasiparticle excitation energies for $N = 6$ and $N = 8$. The states are ordered as $1s_{1/2}$, $1p_{3/2}$, $1p_{1/2}$, $2s_{1/2}$, $1d_{3/2}$, $1f_{7/2}$, $2p_{3/2}$, $2p_{1/2}$, and $1f_{7/2}$, and the energies are indicated by circles.
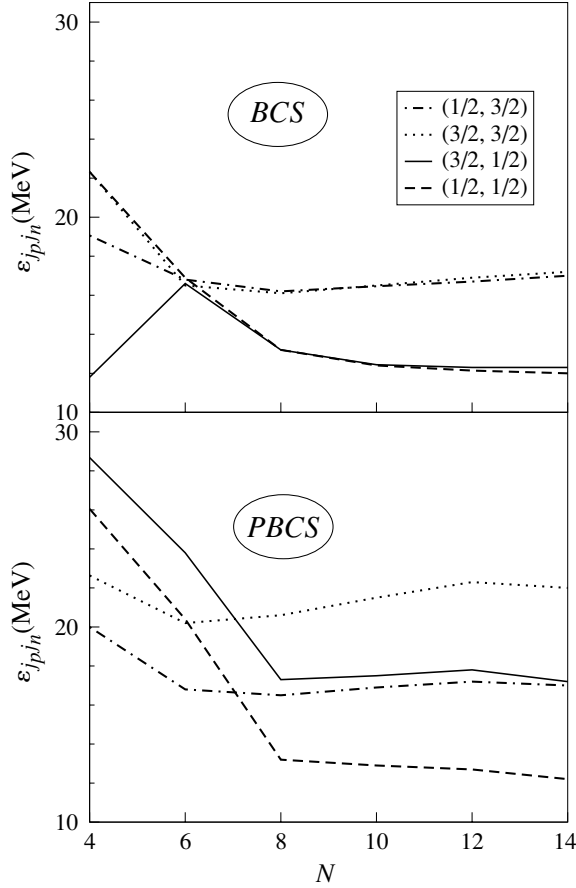
FIG. 2. Unperturbed two-quasiparticle energies $\mathcal{E}_{j_p j_n}$ for nitrogen isotopes, as a function of N, of the states $|1p_{1/2}1p_{3/2}\rangle$, $|1p_{3/2}1p_{3/2}\rangle$, $|1p_{1/2}1p_{1/2}\rangle$, and $|1p_{3/2}1p_{1/2}\rangle$. (Upper panel) BCS results. (Lower panel) PBCS results.

GT strength in ^{12}N, given by

$$S_{\mathrm{GT}}(E) \equiv \frac{1}{\pi} \sum_{pn} |g_A \langle p \| \sigma \| n \rangle|^2 \frac{\eta}{\eta^2 + \left(E - \mathcal{E}_{j_p j_n}\right)^2}. \quad (4.4)$$

The BCS and PBCS results for ^{12}N, when folded with $\eta = 1$ MeV, are compared in Fig. 4. The PBCS energy ordering, given by (4.3), is accompanied by the partial shifting of the GT strength to higher energies. Therefore it can be said that within the PBCS the GT resonance is quenched even at the level of the mean field.

In view of these disadvantages of the standard BCS approach, from now on we will mainly discuss the number projection results. In our previous work [14] we have also pointed out that the values of the coupling strengths v_s and v_t within the pp and ph channels used in $N > Z$ nuclei ($v_s^{\mathrm{pp}} \equiv v_s^{\mathrm{pair}}$ and $v_t^{\mathrm{pp}} \gtrsim v_s^{\mathrm{pp}}$) might not be suitable for $N = Z$ nuclei. In fact, the best agreement with data in ^{12}C was obtained when the pp channel is totally switched off (i.e., $v_s^{\mathrm{pp}} \equiv v_t^{\mathrm{pp}} = 0$) and using three different sets of values for the ph coupling strengths [14], as follows:

Parametrization I (PI): $v_s^{\mathrm{ph}} = v_s^{\mathrm{pair}} = 24$ MeV fm^3 and $v_t^{\mathrm{ph}} = v_s^{\mathrm{ph}}/0.6 = 39.86$ MeV fm^3. This means that the singlet ph strength is the same as v_s^{pair} obtained from the proton and
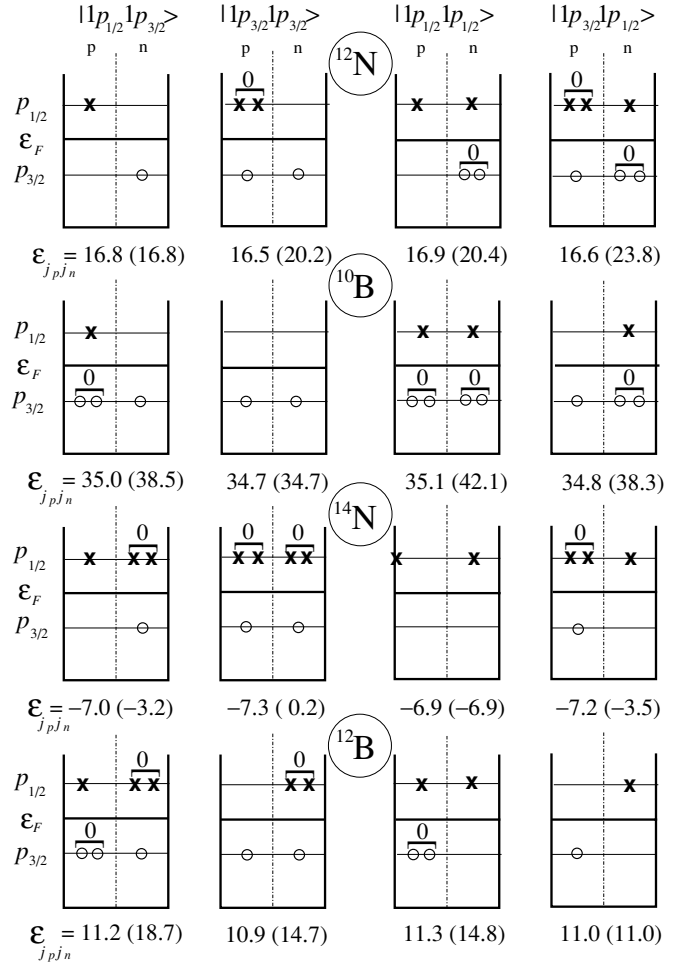

FIG. 3. Schematic representation of the particle-hole limits for the seniority two-pn states. The zero-angular-momentum couplings of two particles or two holes are indicated by a horizontal bracket. $\mathcal{E}_F$ represents the Fermi energy. The unperturbed energies $\mathcal{E}_{j_p j_n}$ are given in MeV, with the PBCS results given in brackets.

neutron gap equations, whereas the triplet ph depth is estimated from the relation used by Goswami and Pal [29] in the RPA calculation of ^{12}C.

Parametrization II (PII): $v_s^{\mathrm{ph}} = 27$ MeV fm^3 and $v_t^{\mathrm{ph}} = 64$ MeV fm^3. These values were first used in Refs. [20,30] and later on in the QRPA calculations of ^{48}Ca [13,24,31].

Parametrization III (PIII): $v_s^{\mathrm{ph}} = v_t^{\mathrm{ph}} = 45$ MeV fm^3. With these coupling constants it is possible to reproduce fairly well the energies of the $J^\pi = 0_1^+$ and 1_1^+ states in ^{12}B and ^{12}N.

The results displayed in Fig. 5 suggest that the choice $v_t^{\mathrm{pp}} = 0$ for the pp parameter in the $S = 0$, $T = 1$ channel could be appropriate for the description of the $N = Z$ nuclei. They are shown as functions of the parameter

$$t = \frac{2v_t^{\mathrm{pp}}}{v_s^{\mathrm{pair}}(p) + v_s^{\mathrm{pair}}(n)},$$

together with the experimental data for (1) the energy difference ω_{1^+} between the 1^+ ground state in ^{12}N and the 0^+ ground state in ^{12}C, (2) the B value for the GT β transition between these two states, and (3) the corresponding exclusive
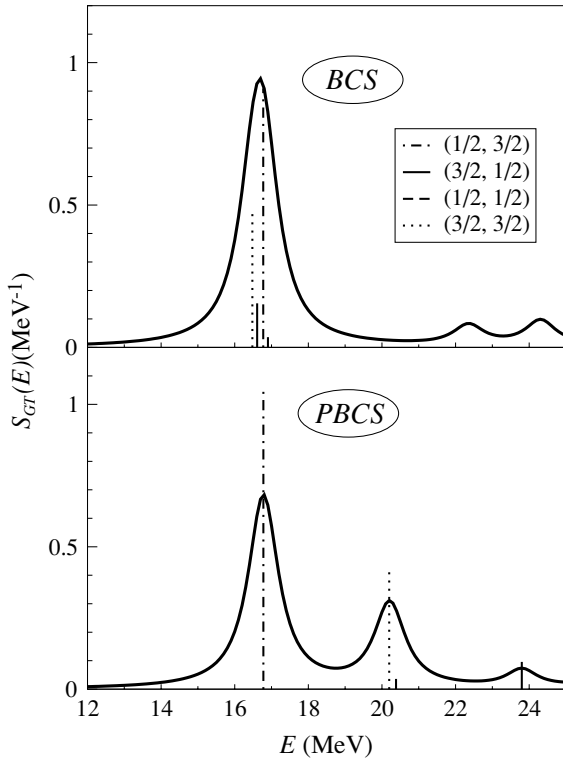
FIG. 4. BCS (upper panel) and the PBCS (lower panel) GT strength functions in ^{12}N.
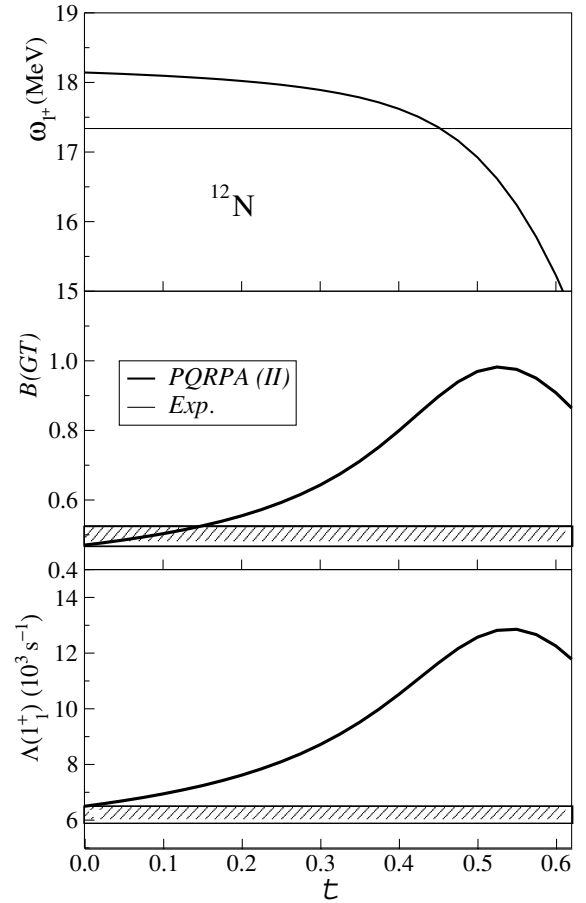

FIG. 5. The results of the PQRPA calculations, as functions of the *pp* parameter t, compared with the experimental data taken from Refs. [27,32,33] for (1) the energy difference ω_{1^+} between the 1^+ ground state in ^{12}N and the 0^+ ground state in ^{12}C (upper panel), (2) the B value for the GT β transition between these two states (middle panel), and (3) the corresponding muon-capture rate $\Lambda(1_1^+)$ (lower panel). The values of $v_s^{\rm ph}$ and $v_t^{\rm ph}$ correspond to PII.

muon-capture rate $\Lambda(1_1^+) \equiv \Lambda^{\rm exc}$. The values of $v_s^{\rm ph}$ and $v_t^{\rm ph}$ are those from the PII, but quite similar results are obtained with the other two sets of parameters. Note that the ph interaction first shifts the energy ω_{1^+} upward by ~ 1.5 MeV, from its unperturbed value $\mathcal{E}_{1p_{3/2}1p_{3/2}} = 16.8$ MeV. Then, when t is increased, we have an opposite attractive effect. That is, the pp interaction diminishes ω_{1^+} up to $t \gtrsim 0.6$, where the well-known collapse of the QRPA approximation occurs. At variance with what happens in the case of heavy nuclei, here the values of $B(GT)$ and $\Lambda(1_1^+)$ basically rise with t, and agreement with the data is achieved only when the pp interaction is totally switched off. Quite generally, the nuclear moments (2.34) also depend weakly on the $S = 1, T = 0$ channel parameter $v_s^{\rm pp}$, for which we adopt as well the null value, just to be consistent with our election of $v_t^{\rm pp}$.

Results for the muon-capture rates and the neutrino (ν_e, e^-) DAR and (ν_μ, μ^-) DIF reaction flux-averaged cross sections are shown, respectively, in Tables V, Tables VI and Tables VII.

The flux-averaged cross section is defined as

$$\overline{\sigma}_\ell(J_f) = \int_{\Delta_{J_f}} dE_\nu \sigma_\ell(E_\nu, J_f) \Phi_\ell(E_\nu), \ \ell = e, \mu, \quad (4.5)$$

where $\Phi_\ell(E_\nu)$ is the normalized neutrino flux. For electron neutrinos this flux was approximated by the Michel spectrum, and for the muon neutrinos we used that from Ref. [37]. The energy integration is carried out in the DAR interval $m_e + \omega_{J_f} \leqslant \Delta_{J_f}^{\rm DAR} \leqslant 52.8$ MeV for electrons and in the DIF interval $m_\mu + \omega_{J_f} \leqslant \Delta_{J_f}^{\rm DIF} \leqslant 300$ MeV for muons.

The full PQRPA calculations, which include relativistic corrections, are listed for all three parametrizations (I, II, and III) whereas, the theoretical results involving just the velocity-independent operators $\mathsf{Y}_J(\kappa\mathbf{r})$ and $\mathsf{S}_{JL}(\kappa\mathbf{r})$ are displayed only for the PII case. Contributions of the other two operators, $\mathsf{P}_{JL}(\kappa\mathbf{r})$ and $\mathsf{Y}_J(\kappa\mathbf{r}, \boldsymbol{\sigma} \cdot \mathbf{v})$, to the muon-capture rates are small (of the order of 5%) as displayed in Table V. The only exception is for the 0^- states, where the relativistic operator $\mathsf{Y}_0(\kappa\mathbf{r}, \boldsymbol{\sigma} \cdot \mathbf{v})$ dominates over the nonrelativistic one $\mathsf{S}_{01}(\kappa\mathbf{r})$. We also see from Tables VI and VII that nonlocality effects on the neutrino-nucleus reactions are of the order of 1% and therefore can be neglected.

The numerical results are sorted according to the order of forbiddenness of the transition moments, which can be *allowed* (A): $J^\pi = 0^+, 1^+$; *first forbidden* (F1): $J^\pi = 0^-, 1^-, 2^-$; *second forbidden* (F2): $J^\pi = 2^+, 3^+$; *third forbidden* (F3): $J^\pi = 3^-, 4^-$; and so on. The response of the three weak processes to successive multipoles is strongly correlated with the average momentum transfer $\overline{\kappa}$ involved in each: For

TABLE V. Experimental and calculated muon-capture rate in units of 10^3 s^{-1}. The full PQRPA calculations, which include the relativistic corrections, are listed for all three parametrizations. Theoretical results that involve only the velocity-independent matrix elements are displayed in parentheses in the third column for the case PII. The rates are grouped by their degrees of forbiddenness. We show (i) the exclusive rates $\Lambda(J^\pi)$, for $J_f^\pi = 1_1^+, 1_1^-, 2_1^-, 2_1^+$, (ii) the multipole decomposition of the rates $\sum_f \Lambda(J_f^\pi)$ for each final state with spin and parity J_f^π, and (iii) the inclusive decay rate $\Lambda^{\mathrm{inc}} \equiv \sum_{J_f^\pi} \Lambda(J_f^\pi)$. In the fourth column are listed the results of recent SM calculations, which are explained in the text. The measured capture rates are given in the last column.

Muon-capture rate	PQRPA			Shell model			Experiment
	(I)	(II)	(III)	SM1 [16]	SM2 [16]	SM3 [17]	
Allowed		49.3%		39.3%			
$\Lambda(1_1^+)$	7.52	6.27(6.50)	6.27	11.56	6.3	6.0	6.2 ± 0.3 [33]
$\sum_f \Lambda(0_f^+)$	3.68	2.86(3.15)	3.77	0.21			
$\sum_f \Lambda(1_f^+)$	20.28	18.14(18.63)	18.22	15.43			
First forbidden		46.6%		55.7%			
$\Lambda(1_1^-)$	1.06	0.49(0.51)	0.98			1.86	0.62 ± 0.20 [34,35]
$\Lambda(2_1^-)$	0.31	0.18(0.18)	0.16			0.22	0.18 ± 0.10 [34,35]
$\sum_f \Lambda(0_f^-)$	2.62	2.35(0.72)	2.35	2.12			
$\sum_f \Lambda(1_f^-)$	11.84	10.37(9.51)	11.37	12.25			
$\sum_f \Lambda(2_f^-)$	7.78	7.12(6.90)	7.15	7.79			
Second forbidden		3.9%		4.6%			
$\Lambda(2_1^+)$	0.19	0.14(0.16)	0.15			0.25	0.21 ± 0.10 [34,35]
$\sum_f \Lambda(2_f^+)$	1.26	1.09(0.89)	1.17	1.36			
$\sum_f \Lambda(3_f^+)$	0.63	0.57(0.57)	0.58	0.46			
Λ^{inc}	48.16	42.56(40.7)	44.67	39.82	41.9	33.5	38 ± 1 [36]

the (ν_e, e^-) reaction, $\overline{\kappa} \sim 0.2$ fm^{-1}; for muon-capture, $\overline{\kappa} \sim 0.5$ fm^{-1}; and for the (ν_μ, μ^-) reaction, $\overline{\kappa} \sim 1$ fm^{-1}. As a consequence, in the first case the A moments are by far the dominant ones, contributing $\sim$83.0%, with the remaining part of the reaction strength carried almost entirely ($\sim$16.6%) by the F1 moments. For muon capture, the A- and F1-matrix elements contribute, respectively, 49.3% and 46.6%, whereas the F2 moments carry only 3.9% of the total transition rate, and the contribution of the F3 moments are negligibly small. Finally, the inclusive cross section in the (ν_μ, μ^-) reaction

TABLE VI. Experimental and calculated flux-averaged cross section for the $^{12}\mathrm{C}(\nu_e, e^-)^{12}\mathrm{N}$ DAR reaction in units of 10^{-42} cm^2. The full PQRPA calculations, which include the relativistic corrections, are listed for all three parametrizations. Theoretical results that involve only the velocity-independent matrix elements are displayed in parentheses for the case PII in the third column. The multipole decomposition $\sum_f \overline{\sigma}_e(J_f^\pi)$ for each final state with spin and parity J_f^π, as well as the exclusive, $\overline{\sigma}_e^{\mathrm{exc}} \equiv \overline{\sigma}_e(J_f^\pi = 1_1^+)$, and inclusive, $\overline{\sigma}_e^{\mathrm{inc}} = \sum_{J_f^\pi} \overline{\sigma}_e(J_f^\pi)$ cross sections, are shown. In the fourth column are listed the results of recent SM calculations, which are explained in the text. The measured cross sections are given in the last column.

(ν_e, e^-) cross section	PQRPA			Shell model			Experiment
	(I)	(II)	(III)	SM1 [16]	SM2 [16]	SM3 [17]	
Allowed		83.0%		83.6%			
$\overline{\sigma}_e(1_1^+)$	9.94	8.07(8.00)	8.17	20.86	7.9	9.3	$8.9 \pm 0.3 \pm 0.9$ [4]
$\sum_f \overline{\sigma}_e(0_f^+)$	1.92	1.35(1.31)	2.01	0.00			
$\sum_f \overline{\sigma}_e(1_f^+)$	15.98	14.08(14.22)	12.14	22.52			
First forbidden		16.6%		16.0%			
$\sum_f \overline{\sigma}_e(0_f^-)$	0.07	0.07(0.05)	0.07	0.04			
$\sum_f \overline{\sigma}_e(1_f^-)$	1.94	1.59(1.43)	1.80	1.90			
$\sum_f \overline{\sigma}_e(2_f^-)$	1.66	1.43(1.41)	1.44	2.36			
Second forbidden		0.4%		0.4%			
$\sum_f \overline{\sigma}_e(2_f^+)$	0.07	0.05(0.04)	0.05	0.08			
$\sum_f \overline{\sigma}_e(3_f^+)$	0.03	0.03(0.03)	0.03	0.03			
$\overline{\sigma}_e^{\mathrm{inc}}$	21.67	18.60 (18.49)	17.54	26.93	12.5	15.1	$13.2 \pm 0.4 \pm 0.6$ [4]

TABLE VII. Same as Table VI but for the averaged exclusive, $\overline{\sigma}_\mu^{\text{exc}} \equiv \overline{\sigma}_\mu(J_f^\pi = 1_1^+)$, and inclusive, $\overline{\sigma}_\mu^{\text{inc}} = \sum_{J_f^\pi} \overline{\sigma}_\mu(J_f^\pi)$, cross sections for the $^{12}\text{C}(\nu_\mu, \mu^-)^{12}\text{N}$ DIF reaction in units of 10^{-40} cm^2.

(ν_e, e^-) cross section	PQRPA			Shell model			Experiment
	(I)	(II)	(III)	SM1 [16]	SM2 [16]	SM3 [17]	
Allowed		20.0%		17.1%			
$\overline{\sigma}_\mu(1_1^+)$	0.74	0.59(0.56)	0.59	1.16	0.56	0.9	$0.56 \pm 0.08 \pm 0.10$ [5]
$\sum_f \overline{\sigma}_\mu(0_f^+)$	0.37	0.26(0.26)	0.39	0.11			
$\sum_f \overline{\sigma}_\mu(1_f^+)$	2.68	2.33(2.40)	2.34	2.95			
First forbidden		39.5%		36.4%			
$\sum_f \overline{\sigma}_\mu(0_f^-)$	0.03	0.04(0.07)	0.04	0.07			
$\sum_f \overline{\sigma}_\mu(1_f^-)$	3.34	2.79(2.84)	3.10	3.55			
$\sum_f \overline{\sigma}_\mu(2_f^-)$	2.53	2.28 (2.13)	2.29	2.91			
Second forbidden		27.1%		22.2%			
$\sum_f \overline{\sigma}_\mu(2_f^+)$	2.55	2.28(2.11)	2.37	2.59			
$\sum_f \overline{\sigma}_\mu(3_f^+)$	1.34	1.23(1.29)	1.23	1.39			
Third forbidden		10.2%		17.7%			
$\sum_f \overline{\sigma}_\mu(3_f^-)$	0.74	0.69(0.73)	0.71	1.77			
$\sum_f \overline{\sigma}_\mu(4_f^-)$	0.68	0.63(0.63)	0.63	1.41			
Fourth forbidden		3.1%		6.5%			
$\sum_f \overline{\sigma}_\mu(4_f^+)$	0.22	0.21(0.20)	0.21	0.66			
$\sum_f \overline{\sigma}_\mu(5_f^+)$	0.20	0.19(0.19)	0.19	0.51			
$\overline{\sigma}_\mu^{\text{inc}}$	14.69	12.94(12.86)	13.51	17.92	13.8	19.2	$10.6 \pm 0.30 \pm 1.80$ [5]

is spread out rather uniformly over several multipoles and it is necessary to include up to fourth forbidden moments, with their intensities distributed as follows: 20.0% (A), 39.5% (F1), 27.1% (F2), 10.2% (F3), and 3.1% (F4). The exclusive contributions, coming from the ground state 1_1^+, are quite different in the three cases owing to the afore mentioned implication of the momentum transfer. That is, of the total transition rates for the (ν_e, e^-) reaction, muon capture, and the (ν_μ, μ^-) reaction, the exclusive contributions are, respectively, 43%, 15%, and 5%.

Let us say a few words on the comparison of our results with the experimental data:

- *Muon capture* (Table V): All exclusive rates $\Lambda(J^\pi)$ with $J_f^\pi = 1_1^+, 1_1^-, 2_1^-, 2_1^+$ are fairly well accounted for by the theory, whereas the inclusive rate, Λ^{inc}, is overpredicted by $\sim$10%.

- (ν_e, e^-) reaction (Table VI): Even though the exclusive cross section, $\overline{\sigma}_e^{\text{exc}}$, is well reproduced within the PQRPA, the inclusive one, $\overline{\sigma}_e^{\text{inc}}$, is $\sim$40% above the data. A plausible explanation for this difference could be the fact that we find a very significant amount of the GT strength (32%) and the Fermi strength (7%) within the DAR energy interval, 18 MeV $\lesssim E_\nu \lesssim$ 50 MeV, where the electron-neutrino flux, $\Phi_e(E_{\nu_e})$, changes very abruptly, making the inclusive cross section very sensitive to the strength distribution of low-lying excited states.

- (ν_μ, μ^-) reaction (Table VII): Here also the exclusive cross section, $\overline{\sigma}_\mu^{\text{exc}}$, is in full agreement with the data, whereas the inclusive one, $\overline{\sigma}_\mu^{\text{inc}}$, is overpredicted by $\sim$20%.

In the last three tables we also confront our PQRPA results with the SM calculations performed by: (a) Hayes and Towner [16], within the model spaces called by them as (iii) and (iv), and which are labeled here, respectively, as SM1 and SM2, and (b) Auerbach and Brown [17], which we label as SM3. The multipole breakdown in the contributions to the cross sections from each multipole is only given for the SM1 scheme [16]. At first glance our results seem to agree fairly well with the SM ones, particularly when the amounts of allowed and forbidden transition strengths are confronted. However, this is not true, as can be seen from a more careful analysis of the multipole structure of the transition rates.

For instance, the total positive parity capture rates with the 1_1^+ state excluded [i.e., $\sum_{J_f \neq 1_1^+} \Lambda(J_f^+)$] are equal to 5.9 and 3.6 in SM1 and SM3, respectively, whereas we get 16.4 (in units of 10^3 s^{-1}). Note also that in SM calculations almost all the GT strength is exhausted by the ground-state transition, whereas within the PQRPA only 35% of this strength goes into the 1_1^+ state. Another important discrepancy is in the Fermi transitions, for which we get $\sum_f \Lambda(0_f^+) = 2.86$, whereas they obtain only $\sum_f \Lambda(0_f^+) = 0.21$ (in units of 10^3 s^{-1}).

One sees that our $\overline{\sigma}_e^{\text{exc}}$ is consistent with the SM2 and SM3 shell model calculations, whereas our $\overline{\sigma}_e^{\text{inc}}$ falls in between the SM1 and SM2 calculations and is $\sim$20% larger than the SM3 result. However, as in muon capture, we find much more $\overline{\sigma}_e(1^+)$ strength in the excited states of the ^{12}N nucleus than appears in SM calculations. Namely, we obtain $\sum_{J_f \neq 1_1^+} \overline{\sigma}_e(J_f^+) = 7.44$, whereas in SM1 and SM3 this quantity is, respectively, 1.77 and 0.40 (in units of 10^{-42} cm^2).
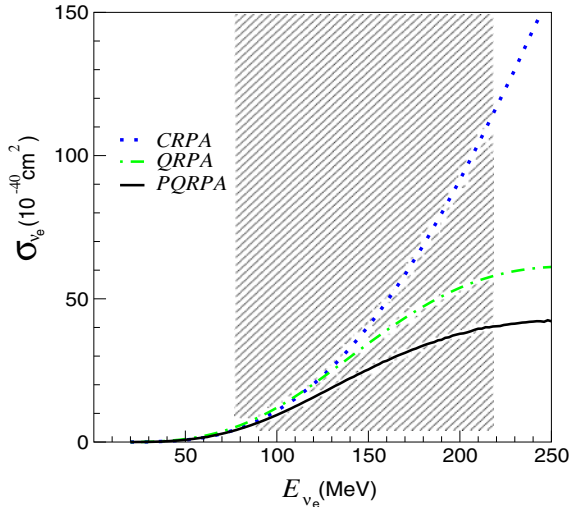
FIG. 6. (Color online) Calculated cross section σ_{ν_e} as a function of the neutrino energy. The dashed region indicates the experimental energy window.

Moreover, in all three SM calculations more than 90% of the $\overline{\sigma}_e(1^+)$ strength is concentrated in the ^{12}N ground state whereas we find only 57%.

In the same way as in the SM calculations, within the PQRPA the total DIF cross section is mainly built up from forbidden excitations. Nevertheless, although the PQRPA results agree with the SM2 calculation, they are quite small when compared with those provided by the SM1 and SM3 models, for both $\overline{\sigma}_\mu^{\mathrm{exc}}$ and $\overline{\sigma}_\mu^{\mathrm{inc}}$. The differences in $\overline{\sigma}_\mu^{\mathrm{inc}}$ come not only from the positive parity contributions but also from the negative parity ones.

As a corollary of this discussion we would like to stress that it is not easy to assess whether the PQRPA results are better or worse than the shell model ones. We can only say that with the use of just a few essentially phenomenological parameters the PQRPA is able to account for a large number of weak processes in ^{12}C. (The experimental energies of the $3/2_1^-$ state in ^{13}C and ^{13}N are also predicted within the PBCS.) That is, the single-particle energies e_j, for $j = 1p_{3/2}, 1p_{1/2}, 1d_{5/2}, 2s_{1/2}, 1d_{3/2}, 1f_{7/2}, 2p_{3/2}$, and the pairing strength v_s^{pair} have been fixed from the experimental energies of the odd-mass nuclei ^{11}C, ^{11}B, ^{13}C and ^{13}N, whereas the particle-hole coupling strengths v_s^{ph} and v_t^{ph} were taken from the previous QRPA calculations of ^{48}Ca [13,24,31]. Only the particle-particle couplings v_s^{pp} and v_t^{pp} have been treated as free parameters, and we have used here $v_s^{\mathrm{pp}} = v_t^{\mathrm{pp}} = 0$. It

would be interesting to inquire whether this rather extreme parametrization is also appropriate for the description of other light $N = Z$ nuclei, such as ^{14}N and ^{16}O, which have been discussed recently within a shell model scheme [17].

Finally, we point out that in the DIF neutrino oscillation search [1] an excess signal of

$$N_{\nu_\mu \to \nu_e}^{\mathrm{exp}} = 18.1 \pm 6.6 \pm 4.0$$

events has been observed in the ^{12}C$(\nu_e, e^-)^{12}$N reaction, which are evaluated theoretically by the expression

$$N_{\nu_\mu \to \nu_e}^{\mathrm{th}} = \int_{\Delta^{\mathrm{osc}}} dE_\nu \sigma_e(E_\nu) P_{\nu_\mu \to \nu_e}(E_\nu) \Phi_\mu(E_\nu),$$

$$\sigma_e(E_\nu) \equiv \sum_{J_f} \sigma_e(E_\nu, J_f),$$

where $77.3 \ \mathrm{MeV} \leqslant \Delta^{\mathrm{osc}} \leqslant 217.3 \ \mathrm{MeV}$ stands for the experimental energy window. The oscillation probability reads

$$P_{\nu_\mu \to \nu_e}(E_\nu) = \sin^2(2\theta) \sin^2\left(\frac{1.27\Delta m^2 L}{E_\nu}\right),$$

where θ is the mixing angle between the neutrino mass eigenstates, Δm^2 is the difference in neutrino eigenstate masses squared, in eV^2, and L is the distance in meters traveled by the neutrino from the source. One sees therefore that the extraction of the permitted values of θ and Δm^2 from experimental data might depend critically on the theoretical estimate of $\sigma_e(E_\nu)$. So far, the electron cross section obtained within the continuum random phase approximation (CRPA) [38] has been used [1]. This $\sigma_e(E_\nu)$ is compared in Fig. 6 with our QRPA and PQRPA results calculated with PII. As can be noticed the PQRPA yields a substantially different $\sigma_e(E_\nu)$, inside the experimental energy window for the neutrino energy. The consequences of this difference on the confidence regions for $\sin^2(2\theta)$ and Δm^2 will be discussed in a future paper.

After finishing this work we have learned that quite recently Nieves *et al*. [39] were able to describe rather well the inclusive muon-capture rate in ^{12}C, and the inclusive ^{12}C$(\nu_\mu, \mu^-)^{12}$N and ^{12}C$(\nu_e, e^-)^{12}$N cross sections, within the framework of a local Fermi gas picture that includes the RPA correlations.

[1] C. Athanassopoulos *et al*. (LSND Collaboration), Phys. Lett. **81**, 1774 (1998); Phys. Rev. C **58**, 2489 (1998).

[2] A. Aguilar *et al*. (LSND Collaboration), Phys. Rev. D **64**, 112007 (2001).

[3] K. Eitel *et al*. (KARMEN Collaboration), Nucl. Phys. B, Proc. (Suppl.) **77**, 212 (1999).

[4] L.-B. Auerbach *et al*. (LSND Collaboration), Phys. Rev. C **64**, 065501 (2001).

[5] L.-B. Auerbach *et al*. (LSND Collaboration), Phys. Rev. C **66**, 015501 (2002).

[6] T. W. Donnelly and W. C. Haxton, At. Data Nucl. Data Tables **23**, 103 (1979); T. W. Donnelly and R. D. Peccei, Phys. Rep. **50**, 1 (1979).

[7] J. D. Walecka, *Theoretical Nuclear and Subnuclear Physics* (Oxford University Press, New York, 1995), p. 531.

[8] N. Auerbach, N. Van Giai, and O. K. Vorov, Phys. Rev. C **56**, R2368 (1997).

[9] C. Volpe, N. Auerbach, G. Colò, T. Suzuki, and N. Van Giai, Phys. Rev. C **62**, 015501 (2000).

[10] T. Kuramoto, M. Fukugita, Y. Kohyama, and K. Kubodera, Nucl. Phys. **A512**, 711 (1990).

[11] J. R. Luyten, H. P. C. Rood, and H. A. Tolhoek, Nucl. Phys. **41**, 236 (1963).

[12] N. Auerbach and A. Klein, Nucl. Phys. **A395**, 77 (1983).

[13] C. Barbero, F. Krmpotić, and D. Tadić, Nucl. Phys. **A628**, 170 (1998); C. Barbero, F. Krmpotić, A. Mariano, and D. Tadić, Nucl. Phys. **A650**, 485 (1999).

[14] F. Krmpotić, A. Mariano, and A. Samana, Phys. Lett. **B541**, 298 (2002).

[15] I. Supek, *Teorijska Fizika i Struktura Materije*, Vol. II, edited by Skolska Knijga, Zagreb, 1964.

[16] A. C. Hayes and I. S. Towner, Phys. Rev. C **61**, 044603 (2000).

[17] N. Auerbach and B. A. Brown, Phys. Rev. C **65**, 024322 (2002).

[18] R. J. Blin-Stoyle and S. C. K. Nair, Adv. Phys. **15**, 493 (1966).

[19] B. A. Brown and B. H. Wildenthal, At. Data Nucl. Data Tables **33**, 347 (1985).

[20] H. Castillo and F. Krmpotić, Nucl. Phys. **A469**, 637 (1987).

[21] F. Osterfeld, Rev. Mod. Phys. **64**, 491 (1992).

[22] I. S. Towner and J. C. Hardy, in *The Nucleus as a Laboratory for Studying Symmetries and Fundamental Interactions*, edited by E. M. Henley and W. C. Haxton (World Scientific, Singapore, 1995), p. 183; nucl-th/9504015.

[23] F. Krmpotić, A. Mariano, T. T. S. Kuo, and K. Nakayama, Phys. Lett. **B319**, 393 (1993).

[24] J. Hirsch and F. Krmpotić, Phys. Rev. C **41**, 792 (1990).

[25] J. Hirsch and F. Krmpotić, Phys. Lett. **B246**, 5 (1990).

[26] F. Krmpotić, J. Hirsch, and H. Dias, Nucl. Phys. **A542**, 85 (1992).

[27] F. Ajzenberg-Selove, Nucl. Phys. **A433**, 1 (1985); TUNL Nuclear Data Evaluation Project, available at www.tunl.duke.edu/nucldata/.

[28] P. J. Siemens and A. S. Jensen, *Elements of Nuclei: Many Body Physics with the Strong Interction* (Addison-Wesley, Redwood City, California, 1987).

[29] A. Goswami and M. K. Pal, Nucl. Phys. **35**, 544 (1962).

[30] K. Nakayama, A. Pio Galeão, and F. Krmpotić, Phys. Lett. **B114**, 217 (1982).

[31] F. Krmpotić and S. Sharma, Nucl. Phys. **A572**, 329 (1994).

[32] D. E. Alburger and A. M. Nathan, Phys. Rev. C **17**, 280 (1978).

[33] G. H. Miller *et al.*, Phys. Lett. **B41**, 50 (1972).

[34] D. F. Measday, Phys. Rep. **354**, 243 (2001).

[35] T. J. Stocki, D. F. Maesday, E. Gete, M. A. Saliba, and T. P. Gorrinde, Nucl. Phys. **A697**, 55 (2002).

[36] T. Suzuki *et al.*, Phys. Rev. C **35**, 2212 (1987).

[37] LSND home page, www.nu.to.infn.it/exp/all/lsnd/.

[38] E. Kolbe, K. Langanke, and P. Vogel, Nucl. Phys. **A652**, 91 (1999).

[39] J. Nieves, J. E. Amaro, and M. Valverde, Phys. Rev. C **70**, 055503 (2004), nucl-th/0408005; nucl-th/0408008; J. E. Amaro, C. Maieron, J. Nieves, and M. Valverde, nucl-th/0409017.